Title

Periscope for noninvasive two-photon imaging of murine retina in vivo.

Journal

Biomedical Optics Express, 6(9)

ISSN

2156-7085

Authors

Stremplewski, Patrycjusz
Komar, Katarzyna
Palczewski, Krzysztof
et al.

Publication Date

2015-09-01

DOI

10.1364/BOE.6.003352

Peer reviewed

Biomedical Optics EXPRESS

Periscope for noninvasive two-photon imaging of murine retina *in vivo*

Patrycjusz Stremplewski,[1] Katarzyna Komar,[1] Krzysztof Palczewski,[2] Maciej Wojtkowski,[1,*] and Grazyna Palczewska[3]

[1]*Institute of Physics, Faculty of Physics, Astronomy and Informatics, Nicolaus Copernicus University in Torun, Grudziadzka 5, 87-100 Torun, Poland*

[2]*Department of Pharmacology, Cleveland Center for Membrane and Structural Biology, School of Medicine, Case Western Reserve University, Cleveland, OH 44106, USA*

[3]*Department of Medical Devices, Polgenix, Inc., Cleveland, OH 44106, USA*

**max@fizyka.umk.pl*

Abstract: Two-photon microscopy allows visualization of subcellular structures in the living animal retina. In previously reported experiments it was necessary to apply a contact lens to each subject. Extending this technology to larger animals would require fitting a custom contact lens to each animal and cumbersome placement of the living animal head on microscope stage. Here we demonstrate a new device, periscope, for coupling light energy into mouse eye and capturing emitted fluorescence. Using this periscope we obtained images of the RPE and their subcellular organelles, retinosomes, with larger field of view than previously reported. This periscope provides an interface with a commercial microscope, does not require contact lens and its design could be modified to image retina in larger animals.

OCIS codes: (170.0110) Imaging systems; (170.4460) Ophthalmic optics and devices; (170.5755) Retina scanning; (180.4315) Nonlinear microscopy; (330.7327) Visual optics, ophthalmic instrumentation.

References and links

1. B. G. Wang, K. Koenig, I. Riemann, R. Krieg, and K. J. Halbhuber, "Intraocular multiphoton microscopy with subcellular spatial resolution by infrared femtosecond lasers," Histochem. Cell Biol. **126**(4), 507–515 (2006).
2. M. Han, G. Giese, S. Schmitz-Valckenberg, A. Bindewald-Wittich, F. G. Holz, J. Yu, J. F. Bille, and M. H. Niemz, "Age-related structural abnormalities in the human retina-choroid complex revealed by two-photon excited autofluorescence imaging," J. Biomed. Opt. **12**(2), 024012 (2007).
3. J. M. Bueno, E. J. Gualda, and P. Artal, "Adaptive optics multiphoton microscopy to study ex vivo ocular tissues," J. Biomed. Opt. **15**(6), 066004 (2010).
4. E. J. Gualda, J. M. Bueno, and P. Artal, "Wavefront optimized nonlinear microscopy of ex vivo human retinas," J. Biomed. Opt. **15**(2), 026007 (2010).
5. J. M. Bueno, A. Giakoumaki, E. J. Gualda, F. Schaeffel, and P. Artal, "Analysis of the chicken retina with an adaptive optics multiphoton microscope," Biomed. Opt. Express **2**(6), 1637–1648 (2011).
6. J. J. Hunter, B. Masella, A. Dubra, R. Sharma, L. Yin, W. H. Merigan, G. Palczewska, K. Palczewski, and D. R. Williams, "Images of photoreceptors in living primate eyes using adaptive optics two-photon ophthalmoscopy," Biomed. Opt. Express **2**(1), 139–148 (2011).
7. R. W. Lu, Y. C. Li, T. Ye, C. Strang, K. Keyser, C. A. Curcio, and X. C. Yao, "Two-photon excited autofluorescence imaging of freshly isolated frog retinas," Biomed. Opt. Express **2**(6), 1494–1503 (2011).
8. G. Palczewska, Z. Dong, M. Golczak, J. J. Hunter, D. R. Williams, N. S. Alexander, and K. Palczewski, "Noninvasive two-photon microscopy imaging of mouse retina and retinal pigment epithelium through the pupil of the eye," Nat. Med. **20**(7), 785–789 (2014).
9. G. Palczewska, M. Golczak, D. R. Williams, J. J. Hunter, and K. Palczewski, "Endogenous Fluorophores Enable Two-Photon Imaging of the Primate Eye," Invest. Ophthalmol. Vis. Sci. **55**(7), 4438–4447 (2014).
10. Y. Imanishi, M. L. Batten, D. W. Piston, W. Baehr, and K. Palczewski, "Noninvasive two-photon imaging reveals retinyl ester storage structures in the eye," J. Cell Biol. **164**(3), 373–383 (2004).
11. G. Palczewska, T. Maeda, Y. Imanishi, W. Sun, Y. Chen, D. R. Williams, D. W. Piston, A. Maeda, and K. Palczewski, "Noninvasive multiphoton fluorescence microscopy resolves retinol and retinal condensation products in mouse eyes," Nat. Med. **16**(12), 1444–1449 (2010).

#244285 Received 3 Jul 2015; revised 1 Aug 2015; accepted 2 Aug 2015; published 13 Aug 2015

12. A. Bindewald-Wittich, M. Han, S. Schmitz-Valckenberg, S. R. Snyder, G. Giese, J. F. Bille, and F. G. Holz, "Two-photon-excited fluorescence imaging of human RPE cells with a femtosecond Ti:Sapphire laser," Invest. Ophthalmol. Vis. Sci. **47**(10), 4553–4557 (2006).
13. M. Han, A. Bindewald-Wittich, F. G. Holz, G. Giese, M. H. Niemz, S. Snyder, H. Sun, J. Yu, M. Agopov, O. La Schiazza, and J. F. Bille, "Two-photon excited autofluorescence imaging of human retinal pigment epithelial cells," J. Biomed. Opt. **11**(1), 010501 (2006).
14. O. La Schiazza and J. F. Bille, "High-speed two-photon excited autofluorescence imaging of ex vivo human retinal pigment epithelial cells toward age-related macular degeneration diagnostic," J. Biomed. Opt. **13**(6), 064008 (2008).
15. Y. Miura, G. Huettmann, R. Orzekowsky-Schroeder, P. Steven, M. Szaszák, N. Koop, and R. Brinkmann, "Two-Photon Microscopy and Fluorescence Lifetime Imaging of Retinal Pigment Epithelial Cells Under Oxidative Stress," Invest. Ophthalmol. Vis. Sci. **54**(5), 3366–3377 (2013).
16. E. A. Boettner and J. R. Wolter, "Transmission of the Ocular Media," Invest. Ophthalmol. **1**(6), 776–783 (1962).
17. G. Palczewska, F. Vinberg, P. Stremplewski, M. P. Bircher, D. Salom, K. Komar, J. Zhang, M. Cascella, M. Wojtkowski, V. J. Kefalov, and K. Palczewski, "Human infrared vision is triggered by two-photon chromophore isomerization," Proc. Natl. Acad. Sci. U.S.A. **111**(50), E5445–E5454 (2014).
18. A. Maeda, G. Palczewska, M. Golczak, H. Kohno, Z. Dong, T. Maeda, and K. Palczewski, "Two-photon microscopy reveals early rod photoreceptor cell damage in light-exposed mutant mice," Proc. Natl. Acad. Sci. U.S.A. **111**(14), E1428–E1437 (2014).
19. R. Sharma, L. Yin, Y. Geng, W. H. Merigan, G. Palczewska, K. Palczewski, D. R. Williams, and J. J. Hunter, "In vivo two-photon imaging of the mouse retina," Biomed. Opt. Express **4**(8), 1285–1293 (2013).
20. F. C. Delori, R. H. Webb, and D. H. Sliney; American National Standards Institute, "Maximum permissible exposures for ocular safety (ANSI 2000), with emphasis on ophthalmic devices," J. Opt. Soc. Am. A **24**(5), 1250–1265 (2007).
21. Y. Geng, L. A. Schery, R. Sharma, A. Dubra, K. Ahmad, R. T. Libby, and D. R. Williams, "Optical properties of the mouse eye," Biomed. Opt. Express **2**(4), 717–738 (2011).
22. F. Helmchen and W. Denk, "Deep tissue two-photon microscopy," Nat. Methods **2**(12), 932–940 (2005).
23. *American National Standard for Safe Use of Lasers Z136.1–2014*, 2007.
24. "Europe and International laser/LED product safety regulations: IEC 60825-1:1993+A1:1997+A2:2001 and IEC 60825-1:2007". 2007.
25. C. J. Jeon, E. Strettoi, and R. H. Masland, "The major cell populations of the mouse retina," J. Neurosci. **18**(21), 8936–8946 (1998).
26. W. Denk, J. H. Strickler, and W. W. Webb, "Two-Photon Laser Scanning Fluorescence Microscopy," Science **248**(4951), 73–76 (1990).
27. G. McConnell, "Improving the penetration depth in multiphoton excitation laser scanning microscopy," J. Biomed. Opt. **11**(5), 054020 (2006).
28. Y. Du, M. Cramer, C. A. Lee, J. Tang, A. Muthusamy, D. A. Antonetti, H. Jin, K. Palczewski, and T. S. Kern, "Adrenergic and serotonin receptors affect retinal superoxide generation in diabetic mice: relationship to capillary degeneration and permeability," FASEB J. **29**(5), 2194–2204 (2015).
29. R. H. Douglas and G. Jeffery, "The spectral transmission of ocular media suggests ultraviolet sensitivity is widespread among mammals," Proc. Biol. Sci. **281**(1780), 20132995 (2014).
30. R. Drabent, K. Bryl, B. Smyk, and K. Ulbrych, "Retinyl palmitate in water environment," J. Photochem. Photobiol. B **37**(3), 254–260 (1997).
31. D. Pestov, Y. Andegeko, V. Lozovoy, and M. Dantus, "Photobleaching and photoenhancement of endogenous fluorescence observed in two-photon microscopy with broadband laser sources," J. Opt. **12**(8), 084006 (2010).
32. E. G. de la Cera, G. Rodríguez, L. Llorente, F. Schaeffel, and S. Marcos, "Optical aberrations in the mouse eye," Vision Res. **46**(16), 2546–2553 (2006).

1. Introduction

Two-photon excited fluorescence (TPEF) imaging of a living eye can reveal details of molecular processes in the retina and retinal pigmented epithelium (RPE). There are a number of native fluorophores which have been reported as sources of fluorescent signals in TPEF retinal imaging: NAD(P)H [1–9], all-*trans* retinol and its derivatives [5, 8–11], retinal condensation products [2, 12–14], melanin [15] and elastin [2]. Moreover, some of these fluorophores undergo chemical changes during the visual cycle. Therefore, monitoring changes in their concentrations in retinal layers could provide insights about the functions of biochemical processes that support vision.

TPEF uses infrared light (IR) in the 700-900 nm wavelength range, a favorable spectral window of light not absorbed by water in the cornea, lens and vitreous [16, 17]. This IR light causes less photochemical tissue damage than visible light of the same exposure duration and power. The longer excitation wavelengths also permit imaging at tissue depths not attainable

#244285 Received 3 Jul 2015; revised 1 Aug 2015; accepted 2 Aug 2015; published 13 Aug 2015

by one-photon fluorescence imaging [18]. Many native fluorophores listed above have absorption bands in ultraviolet/short-visible range that prevent their one-photon excitation *in vivo*.

Two-photon absorption takes place only in a small focal volume; hence fluorophores outside that volume are not excited. Therefore TPEF imaging is based on efficient collection of photons generated in the focal volume and does not require a confocal pinhole to provide a sharp image.

Unfortunately, exposures required for successful *in vivo* imaging both in primates and rodents have been above the safety limits for humans [6, 8, 19]. In some cases, *in vivo* TPEF imaging of retina and RPE in primates [6] and mice [19] with specialized adaptive optics scanning laser ophthalmoscopes (AOSLO) required extremely long acquisition times: 12 and 4 min, respectively. Thousands of individual frames had to be aligned and summed to obtain a single TPEF image. Successful *in vivo* TPEF imaging of the retina and RPE in mouse eye also has been reported [8] using a two-photon microscope equipped with a 75-fs pulsing Ti:Sapphire laser, a dispersion compensation unit and a sensorless adaptive optics system. In this setup, one TPEF frame could be obtained in a short period of time but the level of power at the cornea was also above the safety limit [20]. Thus, optimization of every component of an imaging setup is crucial for safe TPEF imaging *in vivo*.

In this work we report successful TPEF imaging of the retina and RPE in living mice with a newly designed and constructed periscope. This instrument provides an interface with a commercial microscope system and could relatively easily be modified to image the retina and RPE in the eyes of different animal species, including humans. The periscope design also is compatible with sensorless adaptive optics.

2. Methods

Our goal was to develop an optical device that could successfully employ a standard multi-photon fluorescence microscope for *in vivo* imaging of the retina and RPE layer in the eyes of living animals and humans. Realization of this aim required a design and construction of an efficient replacement for the microscope objective and contact lens, as well as diverting the beam by 90° to simulate an arrangement suitable for imaging the human eye fundus. As a proof of concept, the periscope device was designed and after addition to the existing setup, successfully tested. This optical subsystem allowed us to image the retina and RPE layer of a living mouse. The resulting images exhibited a subcellular resolution of the RPE without any discernable damage to retinal structures.

Imaging with Leica TC SP5 confocal MP system

For imaging we used a Leica TCS SP5 confocal MP system (Wetzlar, Germany) equipped with an upright DM6000 CFS stand. The whole system is shown in Fig. 1(a). TCS SP5 was equipped with tunable Chameleon Vision-S laser with dispersion compensation (Coherent, Santa Clara, California). The laser delivered 75 fs laser pulses at an 80 MHz pulse repetition frequency. For imaging purposes, the two-photon excited fluorescence was directed in a non-descanned manner to an external Leica HYD detector with active cooling. The excitation beam was separated from the fluorescence signal by a dichroic mirror DM1 and a blocking filter SPF:Chroma SP680 (Chroma Technology Corp., Bellows Falls, Vermont). Spectral data were obtained with internal HYD detectors (Leica Microsystems, Inc.) in the descanned configuration. In this setup, light emitted from the sample was collected by the internal HYD detector after passing through a prism which split the light into a spectrum ranging from 400 to 700 nm. The imaging speed was 400 lines per second. Each image independent of zoom was 512x512 pixels. For RPE images presented in this paper, 3-4 image frames were averaged but no frame averaging was used for imaging retinal capillaries. Moreover, there was no post-processing of the images.

#244285 Received 3 Jul 2015; revised 1 Aug 2015; accepted 2 Aug 2015; published 13 Aug 2015

2.1 Requirements for the periscope

The new periscope had to fulfill several requirements

Beam diameter, resolution and optical power. The mouse eye focal length and pupil size vary with age and strain of the mouse. The average size of the dilated pupil is about 2 mm [21]. To obtain an image of the best possible quality we used a 2.4 mm beam to avoid underfilling [22] of the pupil and the associated reduction in numerical aperture available for imaging. Optical resolution of the system strongly depends on the eye lens condition. Theoretical value of the optical resolution for excitation beam is 1.2 μm and the depth of focus is 3 μm. Real resolution and axial sectioning is expected to be higher since TPF is nonlinear and the signal comes from the regions of the focal spot of the highest intensity.

In future design for humans, the beam diameter should be about equal to or slightly smaller than the pupil diameter, to use the maximal available NA of the human eye and ensure that all permissible laser power [23, 24] is delivered to the retina for imaging. In order to demonstrate high quality TPF images obtained in decent imaging time of 6s we illuminated mouse eye with optical power of more than 20mW, which is less than one order of magnitude than Maximum Permissible Exposure for the retina. For this estimation we assumed that the MPE for mouse imaging can be obtained by scaling the human MPE using the square of the ratio of the numerical apertures of human (0.22) and mouse (0.49) eyes. Nevertheless we did not detect any changes in the mouse RPE. This agrees with Delori at al. 2007, where it is stated that safety limits were set at least 10 times lower than the damage thresholds. This result also is consistent with data presented in Palczewska at al. 2010 [11].

Field of view. To image most of the interesting RPE areas, about 20°-30° (1 mm-1.5 mm) [25] is required, and this criterion defines the minimum field of view (FOV) for the periscope. The upper limit for the field of view is dictated by the dimensions of the optical elements. Here it is crucial to find a compromise between the field of view and the thickness of the optical elements. A large field of view requires optical elements with large diameters and thickness. A longer optical path through glass components could cause loss of the fluorescence signal, an increase in the system dispersion beyond the capabilities of the dispersion compensation unit and a consequent increase in pulse duration, thereby reducing the efficiency of multi-photon excitation [26].

2.2 Design of the periscope

The input beam for the periscope is the beam at the point of the rear aperture of the microscope objective, and the measured diameter ($1/e^2$) of our beam at that point was about 18 mm. The position of the scanners' pivot point (focal plane of the microscope tube lens) was located 27 mm outside the microscope's body. This parameter was estimated both by finding the stationary point during scanning with a maximum range (the objective was removed from the microscope), and measuring the length of the original Leica adapter for the microscope objectives. A schematic of the periscope that reduced the diameter of the beam by a factor of 7.5 and diverted the optical axis by 90° is presented in Fig. 1(b).

#244285 Received 3 Jul 2015; revised 1 Aug 2015; accepted 2 Aug 2015; published 13 Aug 2015

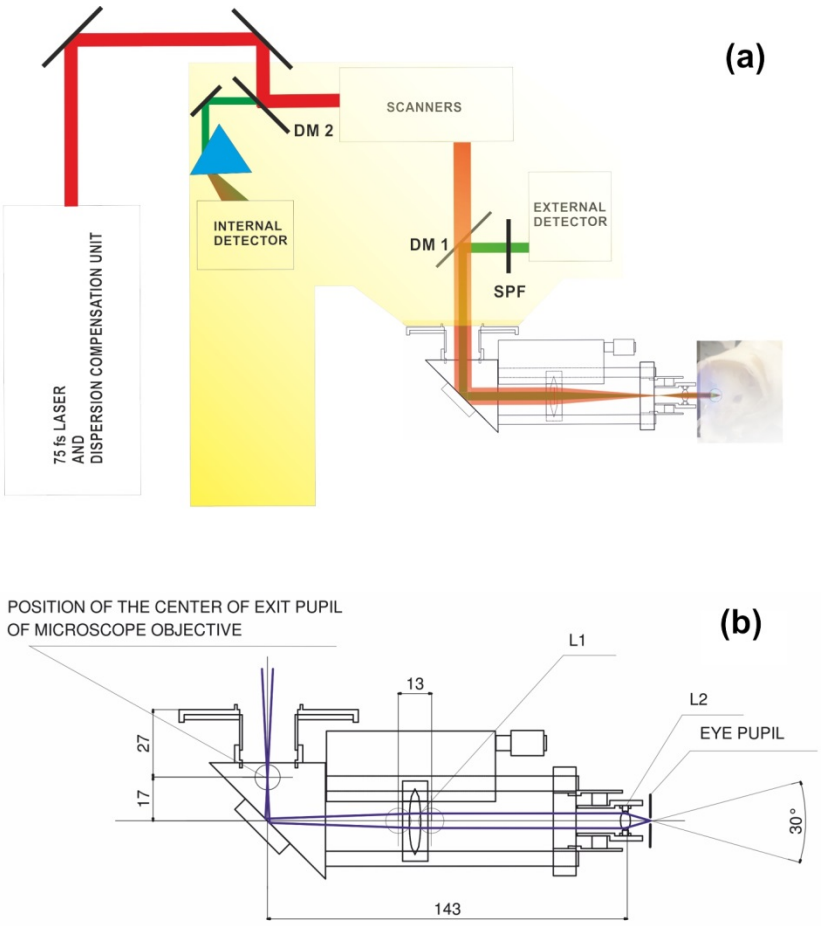

Fig. 1. (a) Position of the periscope in the microscope setup. DM 1 and DM 2 are dichroic mirrors, SPF is a short pass filter. (b) Schematic of the periscope and centers of the extreme rays (blue lines). L1 is an achromatic doublet with a 75 mm focal length and 25 mm diameter; L2 is an achromatic doublet with a 10 mm focal length and an 8 mm diameter. Unless otherwise specified, all dimensions shown are in millimeters.

L1 and L2 are achromatic doublets with focal lengths of 75 mm and 10 mm and diameters of 25 mm and 8 mm, respectively. The optical axis is deviated by 90° with a silver coated mirror. The position of L1 can be changed along the optical axis within a 13 mm range. Changing the position of L1 also changes the position of the focal point along the optical axis inside the eye to focus on a retinal layer of interest. The lens L1 collimates the beam so that lens L2 focuses the beam at its nominal focal length of 10 mm. An L1 shift toward the eye (to the right in Fig. 1) results in a divergent beam at the device output and a focal spot located further away from the anterior segment of the eye, whereas the opposite shift of L1 results in a focal spot located closer to the front of the eye. The same approach can be used to design a periscope for humans. This design provides a collimated beam of 6.3 mm ($1/e^2$) diameter at the output and a FOV of 18°. Adapting the mouse design to humans would include replacing L1 with a lens having a focal length of 100 mm and replacing L2 with a lens with a focal length equal to 35 mm. Results of calculations for imaging depth adjustment, performed by using geometrical optics, are presented in Fig. 2(a). We assumed that the focal length of a mouse eye lens is 2.5 mm [21], and that zero displacement of L1 (the collimated beam at the device output) corresponds to the focal spot placed in the eye 2.5 mm from the cardinal plane of the eye's optical system. The calculated imaging depth adjustment range is about 0.9 mm,

#244285 Received 3 Jul 2015; revised 1 Aug 2015; accepted 2 Aug 2015; published 13 Aug 2015

sufficient to compensate for mouse eye to eye variability and to scan the entire thickness of the retina (for humans this adjustment range is 4 mm). Calculated accuracy of the depth adjustment resulting from the exactness of L1 positioning is below 1 μm.

The goal of our mouse instrument was to obtain RPE images with wide field of view (FOV). However, the FOV changes when the focal spot is shifted. The FOV as a function of the position of focal spot with respect to the cardinal plane of the eye lens is presented in Fig. 2(b).

Considering that the lens of mouse eye is very thick compared to the eye structures dimensions, we expect substantial differences between our model and the real situation. Thus, we treat the results of presented calculations as rough approximations. But in the case of the human eye such a simple model might provide a reasonably good approximation of the actual situation.

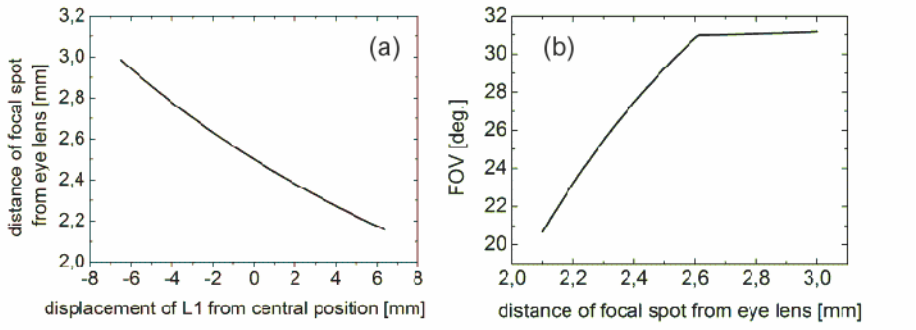

Fig. 2. (a) Calculated imaging depth adjustment range. The central position of L1 results in a collimated periscope output beam and a focal spot located 2.5 mm from eye lens. (b) Calculated FOV versus position of focal spot with respect to the cardinal plane of the eye lens.

2.3 Mice

All animal procedures and experiments used throughout this work were approved by the Institutional Animal Care and Use Committee at Case Western Reserve University and conformed to recommendations of both the American Veterinary Medical Association Panel on Euthanasia and the Association for Research in Vision and Ophthalmology. *Rpe65*$^{-/-}$ mice were generated and genotyped as previously described [11]. C57BL//6J–Tyr^{C-2J} mice were purchased from The Jackson Laboratory. All mice used in this study were between 1- and 6 months old. Housed in the animal facility at the School of Medicine, Case Western Reserve University, they were provided with a regular mouse chow diet and maintained in a 12 h light (~10 lux)/12 h dark cyclic environment. Euthanasia was performed in compliance with the American Veterinary Medical Association (AVMA) Guidelines on Euthanasia, and approval by the Case Western Reserve University Institutional Animal Care and Use Committee. Before imaging mice were housed in regular room light, <20 lux, and did not receive any pharmacological treatments. In preparation for imaging, mouse pupils were dilated with 1% tropicamide and mice then were anesthetized with an intraperitoneal injection of a solution consisting of ketamine (15 mg/ml), xylazine (3 mg/ml) and acepromazine 0.5 mg/ml diluted with water at a dose of 10 μl/g body weight. During imaging the cornea was kept hydrated with Systane eye lubricant drops (Alcon, Fort Worth, TX). To maintain a thin, uniform layer, any excess of the Systane drops was removed with Kimwipes task wipers (Kimberly-Clark, Roswell GA).

#244285 Received 3 Jul 2015; revised 1 Aug 2015; accepted 2 Aug 2015; published 13 Aug 2015

3. Results

3.1 Image optimization

For a periscope dedicated to TPEF imaging, it was critical to compensate its dispersion. As the amount and type of glass in a standard microscope objective and our device differed, we had to obtain new group dispersion delay (GDD) curves and adjust the dispersion compensation unit of the microscope setup to compensate for the new GDD. This procedure was performed by maximizing the TPEF signal emanating from a piece of paper. During the adjustment, a thin lens (f = 8 mm and 4 mm thick) was placed in front of the periscope to focus the excitation beam and to collect TPEF. The excitation pulse duration was 75 fs and we calculated pulse broadening from this thin lens to be below 1 fs [27], allowing the omission of an additional lens. To use the microscope software generated scale bars in images taken with our device, we rescaled the default values. Assuming that the scale bars are added when software is set to use a microscope objective 20x, and that the focal length of this objective (f_{obj}) is 10 mm, the angular magnification of the periscope is:

$$M_a = \frac{f_{L1}}{f_{L2}} = \frac{75}{10} \tag{1}$$

Here, f_{L1} and f_{L2} are the focal lengths of L1 and L2.

The scanning area reduction due to the different focal lengths of the microscope objective and mouse eye (f_{eye}) is:

$$M_f = \frac{f_{eye}}{f_{obj}} = \frac{2.5}{10} \tag{2}$$

Total magnification (scaling factor) is equal to: $M_a x M_f \cong 1.9$. This means that the correct distance is the result indicated by the software multiplied by 1.9. Verification of the scaling factor estimation was performed by imaging a ruler in the focal plane of a lens with a focal length of 19 mm, when the microscope software was set to operate with a microscope objective 20x. Software generated scale recognized a 1 mm distance as 70.7 μm, and the scaling factor obtained from Eqs. (1) and (2) is equal to: $\frac{75}{10}\frac{19}{10} = 14.25$. This results in a distance equal to 1.007 mm, which is close to the real value and confirms the feasibility of using our microscope software-generated scale.

3.2 Imaging of the retina and RPE

The new periscope enabled us to obtain crisp images of the retina and RPE in a living mouse eye. Spatial arrangement of the illumination beam and mouse eye is shown in Fig. 3(a). In this image the 730 nm beam was replaced by blue light for illustration purposes. The design of the periscope placed the pivot point of the scanners at the entrance pupil plane of the mouse eye which produced wide field view (up to ~23° in Fig. 3(b)) images of the RPE and retina. Using two-photon microscope with newly designed and integrated periscope and a laser delivering 75 fs pulses, we imaged the RPE and retinal vasculature in live albino 2.5 month-old WT mice and 3-month-old *Rpe65*$^{-/-}$ mice. The enlarged two-photon images of RPE of albino *Rpe65*$^{-/-}$ and WT mice are shown in Fig. 3(c) and Fig. 3(d), respectively. Individual RPE cells are clearly visible because retinosomes, which store retinyl esters and are located predominantly next to cell membranes, fluoresce upon two-photon excitation [10]. *Rpe65*$^{-/-}$ mice store increased amounts of retinyl esters in their inflated retinosomes [8, 9, 11]. This is consistent with the brighter retinosomes visible at the cell membranes in Fig. 3(c) but not in Fig. 3(d). The size of RPE cells in mice is about 25-30 μm [8, 11] in agreement with cell size evaluated from the scale bars in our figures. The bright spot in the RPE of a WT

#244285 Received 3 Jul 2015; revised 1 Aug 2015; accepted 2 Aug 2015; published 13 Aug 2015

mouse is most probably indicative of a dying RPE cell. The darker shadows visible in Fig. 3(b) originate from the retinal vasculature.

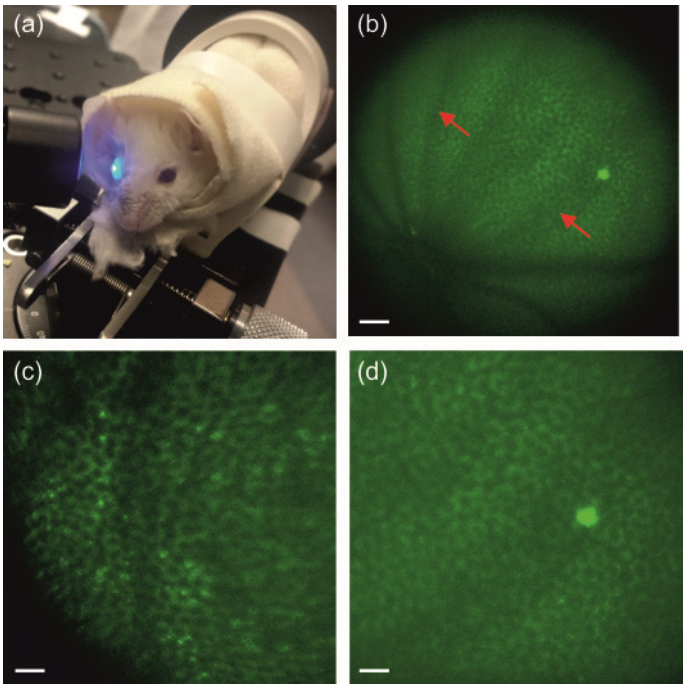

Fig. 3. Two-photon imaging of the RPE in living WT and *Rpe65*$^{-/-}$ mice. (a) Mouse eye illuminated with the newly designed periscope. (b) Image of the RPE in the *WT* albino mouse. (c), (d). Enlarged images of the RPE in *Rpe65*$^{-/-}$ (c) and WT (d) albino mice. Excitation wavelength: 730 nm. Mean power at the cornea: 20 mW in (c) and 25 mW in (b) and (d). Scale bars: 100 µm in (b), and 50 µm in (c) and (d). Red arrows indicate shadows from retinal vasculature.

3.3 Visualization of retinal capillaries by two photon fluorescence

To visualize retinal vasculature in living 2.5-month-old WT mice, sterile FITC-bovine serum albumin (BSA) was injected into their tail veins 30-40 min before imaging [28]. Clear images of retinal vasculature and capillaries were obtained through the animal's eye pupil - Fig. 4. The design of the periscope was optimized to image RPE. Changing the position of focus from the RPE to retinal capillaries resulted in a decreased FOV, hence a non-uniform appearance. Images of capillaries were easier to obtain with a 780 nm than an 800 nm excitation wavelength. To verify optimal settings for our dispersion compensation and confirm that images were formed in response to two-photon excitation, we measured mean gray pixel values for images obtained with and without dispersion compensation (DC). The average ratio of mean pixel gray values acquired with DC to those without DC was 5.5 with a standard deviation equal to 0.9 at both wavelengths. Thus we confirmed that these images were formed in response to two-photon excitation.

#244285 Received 3 Jul 2015; revised 1 Aug 2015; accepted 2 Aug 2015; published 13 Aug 2015

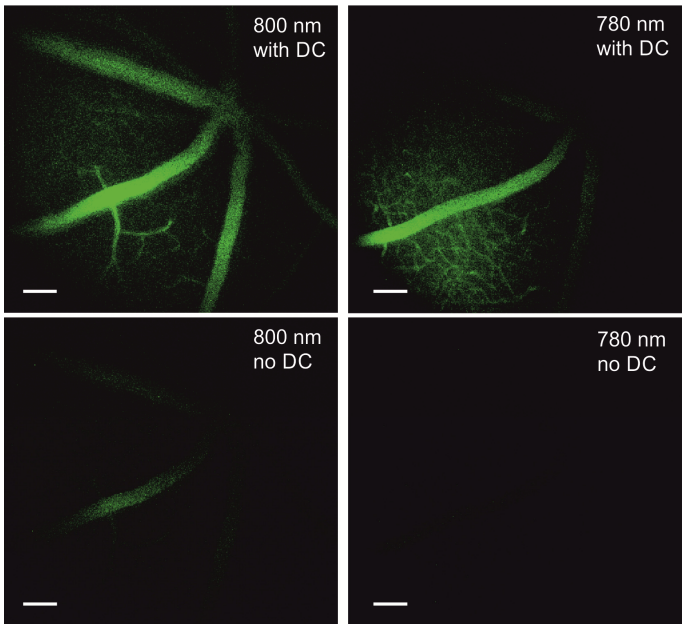

Fig. 4. Images of retinal capillaries in a live WT mouse after tail vain injection with FITC-BSA. Images were acquired with a TPM equipped with a periscope. Top row images were acquired with dispersion compensation (DC), bottom row images were procured without dispersion compensation. Excitation wavelengths are indicated in each image. Scale bars are equal to 100 μm.

3.4 Two photon fluorescence emission spectrum measured in vivo

The signal from the eye of a living *Rpe65*$^{-/-}$ mouse was high enough to obtain a two photon fluorescence emission spectrum with excitation at 730 nm – Fig. 5(a). To obtain spectral components in measured emission spectrum we performed deconvolution after filtration of the spectrum with ocular transmission of mouse eye, Fig. 5(b).

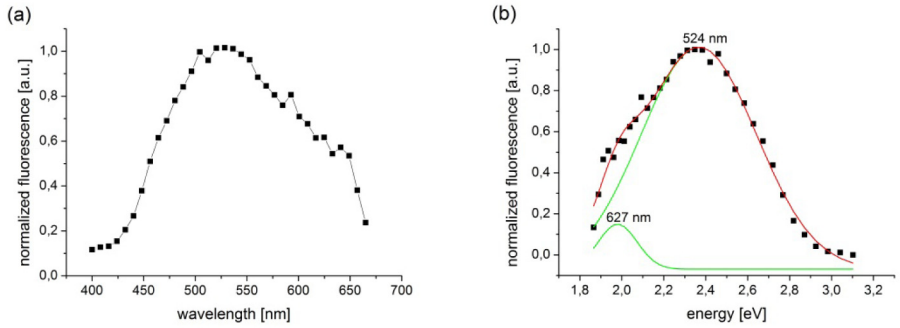

Fig. 5. Fluorescence emission spectrum from the RPE of a live *Rpe65*$^{-/-}$mouse. (a) Spectrum measured with a periscope had maximum at 524 nm. (b) Deconvolution of the spectrum (black squares, red line) revealed two components (green lines), one with a maximum at 524 nm and the second, a long wavelength shoulder with a maximum at 627 nm.

Transmission curves obtained from rodents increase from 0 at 300 nm to almost 1 at 450 nm for young animals [29]. For 90-day-old mice (used in this experiment) the transmission curve had a value of 50% for 315 nm [29] and for the shortest wavelength in our spectrum – 400 nm – about 95-98%. Filtration of the spectrum with a simulated transmission curve did not substantially change the position of the peaks after convolution. The spectrum covered

#244285 Received 3 Jul 2015; revised 1 Aug 2015; accepted 2 Aug 2015; published 13 Aug 2015

almost all the visible region, with a maximum at 524 nm and shoulder around 627 nm, in agreement with previous studies [8]. The maximum emission probably originates from retinyl esters [11]. The environment and propensity of retinyl esters to aggregate could have contributed to the shoulder at longer wavelengths [30].

4. Discussion

The main advantage of the periscope is that it can be applied to large animals contrary to a configuration with a microscope objective. Additionally, as compared to a previous report [8], we obtained images of the RPE with a larger field of view. The procedure for designing the periscope, as described in Methods, is appropriate for microscopes made by different manufacturers. The drawback of the periscope configuration for mice is a smaller field of view in layers outside of the RPE.

The method described here indicates a solution to the ergonomic problem of imaging the eye in larger animals and ultimately humans. When translating two-photon imaging to the human retina, we will need to reduce the exposure levels to below the MPE [23, 24]. A reduction of the light exposure needed for imaging should be possible after incorporating a laser delivering even shorter pulses [26] coupled light with achromatizing lens and advanced pulse shaping methods such as Multiphoton Intrapulse Interference Phase [31] Another strategy would be to reduce light intensity using longer acquisition times and improved image alignment techniques [6]. Considering that optical aberrations introduced by the optics of the mouse eye [32] cause a decrease in the average signal and dynamic range of two-photon images [6] further improvement can be achieved by incorporation of adaptive optics (AO) scanning laser ophthalmoscopy (SLO).

High-resolution noninvasive imaging has become an essential method for understanding complex biological systems in tissues and live animals. Such imaging allows assessment of how biological processes are impacted by disease and therapeutic interventions. Specifically, TPEF retinal imaging *in vivo* is helpful for investigating mechanisms of retinal diseases and developing ophthalmic therapies. Endogenous fluorophores that participate in the retinoid cycle, a process required to replenish visual chromophore and sustain vision, have absorption maxima ranging from 320 – 380 nm. However, the anterior segment of the human eye transmits light poorly at those wavelengths. Two-photon excitation fluorescence imaging employing 75 fs laser pulses overcomes this barrier by allowing visualization of subcellular organelles in the living animal eye at longer excitation wavelengths. Previously reported systems for two-photon imaging of living animal eye required application of a custom contact lens. Here we demonstrate that a newly designed periscope is capable of obtaining high quality TPEF images of the RPE in live mice without custom contact lenses. The instrument provides an interface with a commercial microscope system and could easily be modified to image the retina and RPE in the eyes of different animal species and ultimately humans.

Acknowledgments

We thank Dr. Leslie T. Webster Jr. for helpful comments on this manuscript. We also thank to Dr. Maciej Nowakowski for his valuable comments and remarks. This work was supported by funding from the National Institutes of Health EY025451 (KP), EY021126 (KP), EY024864 (KP), AG043645 (GP) and the Arnold and Mabel Beckman Foundation. This work was also supported by the TEAM project financed by European Union within the framework of Innovative Economy coordinated by Foundation for Polish Science (PS, KK and MW). We would also like to thank Dr. Timothy Kern for enabling the tail vein injections and Dr. Zhiqian Dong for superb mice handling. K.P. is CSO of Polgenix and John H. Hord Professor of Pharmacology.

#244285 Received 3 Jul 2015; revised 1 Aug 2015; accepted 2 Aug 2015; published 13 Aug 2015